Energy distribution and flux of fast neutrals and residual ions extracted from a neutral beam source

Alok Ranjan, Vincent M. Donnelly,[a] and Demetre J. Economou[b]
Plasma Processing Laboratory, Department of Chemical and Biomolecular Engineering, University of Houston, Houston, Texas 77204-4004

(Received 21 April 2006; accepted 6 July 2006; published 7 August 2006)

The energy distribution and flux of the fast neutrals and residual ions extracted from a neutral beam source were measured. Positive ions generated in an inductively coupled argon plasma were extracted through a metal grid with high aspect ratio holes. Ions suffered grazing angle collisions with the inside surface of the grid holes, turning into fast neutrals. The neutral energy distribution was always shifted to lower energies compared to the corresponding residual ion energy distribution. The neutralization efficiency increased with power, decreased with boundary voltage and, for thin neutralization grids, was almost independent of plasma gas pressure. The residual ion flux decreased with increasing hole diameter and hole aspect ratio. The fast neutral flux first increased and then dropped as the hole diameter was increased. Results were explained based on plasma molding inside the grid holes. © *2006 American Vacuum Society.*
[DOI: 10.1116/1.2244537]

I. INTRODUCTION

Charging damage during conventional plasma processing can be a severe problem in microelectronic device fabrication. Because plasma electrons are essentially isotopic and ions are highly anisotropic, high aspect ratio features on a silicon wafer can acquire negative charge on the sidewalls and positive charge on the bottom. This differential charging can divert oncoming positive ions causing etch artifacts such as notching, sidewall bowing, trenching, etc.[1–4] Charging can also result in reduction of the ion flux as a function of depth during etching of high aspect ratio features, leading to aspect ratio dependent etching.[5]

Kuwano and Shimokawa[6] and Shimokawa *et al.*[7] proposed the use of neutral beam etching (NBE) instead of reactive ion etching (RIE) to minimize or avoid charging damage. However, for NBE to be a viable alternative, the neutral beam energy and flux need to be comparable to those in RIE. Earlier designs[8–12] of neutral beam sources suffered from low etch rates. More recently, Panda *et al.*[13] and Samukawa and co-workers[14–16] used an inductively coupled source to obtain a high density plasma. Ions were extracted through a grid with high aspect ratio holes and underwent grazing angle collisions with the internal surfaces of the holes to become fast neutrals. Etch rates observed by these authors were higher than in previous reports. Samukawa and co-workers[14–16] also performed diagnostics of the neutral beam, in an effort to characterize the flux and energy of the fast neutrals and to measure the neutralization efficiency of the extracted ions. They assumed that the fast neutral energy distribution (NED) was the same as the measured residual ion energy distribution (IED). This assumption may be reasonable for glancing angle collisions of ions with atomically smooth surfaces. However, given that the surface of the grid holes may be rough, that the holes can taper because of erosion, and that holes act as lenses to increase the angular spread of the incoming ions (plasma molding[17]), the actual NED and flux must be measured to better characterize the neutral beam source.

Here we report measurements of energy distributions of fast neutrals as well as residual ions in a beam extracted through a grid with high aspect ratio holes. After repelling residual ions, a pulsed electron beam was crossed with the fast neutral beam, ionizing a small fraction of the neutrals. The ionized fast neutrals were dispersed by a parallel-plate energy analyzer and detected by a channel electron multiplier to obtain the energy distribution and relative flux of fast neutrals. The energy distribution and relative flux of residual ions were also measured as a function of the potential on the electrode for accelerating ions (boundary voltage), power input to the plasma, diameter of the grid holes, aspect ratio of the grid holes, and pressure in the plasma.

II. EXPERIMENT

A. Plasma source

The neutral beam source (Fig. 1) was similar to that of Panda *et al.*[13] The inductively coupled plasma (ICP) was ignited in a 1.25 in. inside diameter, 3.25 in. long alumina tube. The 13.56 MHz radio frequency (rf) power (OEM-6, ENI Power Systems) was delivered to the three-turn coil through a matching network. The matching network consisted of two variable capacacitors, C_s and C_p, in series and in parallel to the rf power supply, respectively. The alumina tube and induction coil were immersed in a cooling-jacket circulating de-ionized water at 19 °C. Argon was introduced at the top of the ICP and was regulated by a mass flow controller (model UFC-1000, Unit Instruments).

Ions generated in the plasma source were accelerated out of the plasma by a "beam acceleration electrode" (aluminum)

[a]Electronic mail: vmdonnelly@uh.edu
[b]Electronic mail: economou@uh.edu

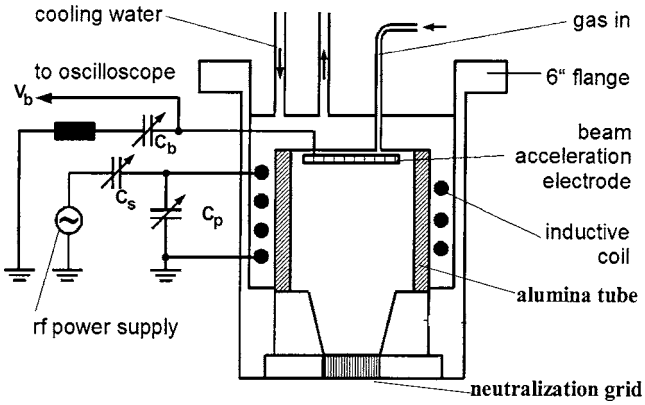

FIG. 1. Schematic of the neutral beam source.

attached to the top of the ICP source. The beam acceleration electrode taps a fraction of power from the rf power supply. A boundary voltage (V_b) was generated by coupling the beam acceleration electrode to the rf power supply by a variable capacitor (C_b). By changing C_b, the boundary voltage V_b could be varied, which provided control over ion energy and hence neutral beam energy. A high voltage divider probe (Tektronix) was used to measure V_b. The accelerated ions pass through a grounded neutralizion grid (Fig. 2), strike the internal surfaces of the holes of the grid at grazing angles, and are converted to fast neutrals. Neutralization grids with four different hole sizes and aspect ratios were used (see Table I). Low pressure in the plasma source (large mean free path) minimized the probability of charge exchange collisions between ions and slow neutrals.

The vacuum system, downstream ultrahigh vacuum (UHV) stainless steel chamber, and associated electronic components are shown schematically in Fig. 3. The downstream chamber housed the sensor for fast neutral and residual ion beam characterizations. The chamber was pumped by a 600 l/s turbomolecular pump (model ET600WS, Ebara Corp.), backed by a two-stage rotary mechanical pump (model CFS 16/25, Leybold). The pressure in the downstream chamber was monitored by an ionization gauge (model G100F, Kurt J. Lesker). With a typical pressure of 10 mTorr in the plasma source (measured by a capacitance manometer, Baratron 626A, MKS), the downstream chamber pressure was $\sim 10^{-5}$ Torr.

TABLE I. Specification of the grids used.

Grid	Hole size (μm)	Pitch (μm)	Transparency (%)	Hole aspect ratio
1	154	272	29	7:1
2	330	470	43	7:1
3	330	470	43	10:1
4	630	914	43	10:1

B. Electron gun

An electron gun (model ELG-2/EGPS-1022, Kimball Physics) was used to ionize the fast neutrals exiting the neutral beam source. The electron gun was operated to deliver a maximum electron current of 10 μA, with an approximate spot size of the electron beam of 2 mm. The energy of the electron beam was fixed at 85 eV to maximize the signal since the electron impact ionization cross section of Ar is maximum at 85 eV.[18] A pulse generator (model 8013B, HP) was used to pulse the electron gun at a frequency of 200 Hz.

C. Parallel-plate electrostatic analyzer

To measure the fast neutral energy distribution, residual ions exiting the neutral beam source were repelled by a grid (Ni, 90% open) at positive potential, 5 mm from the neutralization grid. Another grid (Ni, 90% open) at ground potential 2 mm below shielded the repelling grid and prevented distortion of the electron beam. After passing through the grids, neutrals were ionized by electron impact ionization using the electron gun. The magnitude of the ionized fast neutral current was of the order of picoamperes. It was desirable to analyze ions generated by electron impact of fast neutrals as close to the ionization region as possible to avoid collisions of these ions with background slow neutrals. An inclined parallel-plate electrostatic energy analyzer (called parallel-

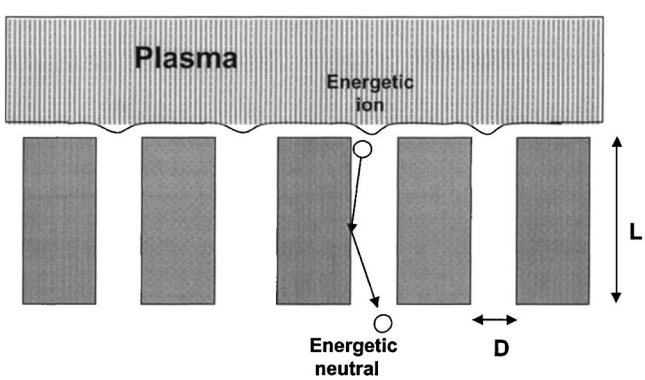

FIG. 2. Schematic of the neutralization grid holes and plasma molding over the holes.

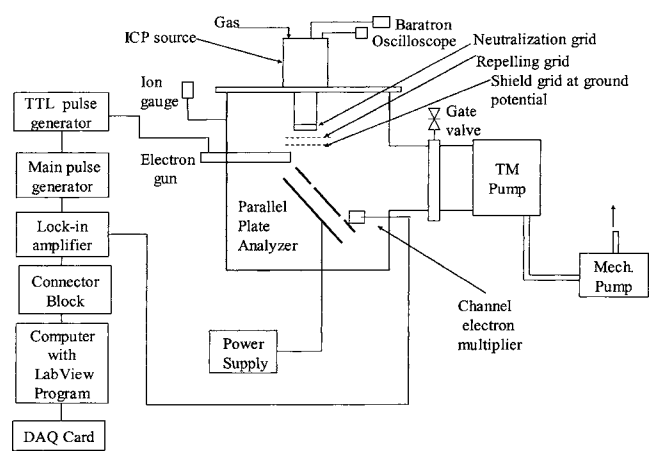

FIG. 3. Schematic of overall experimental setup.

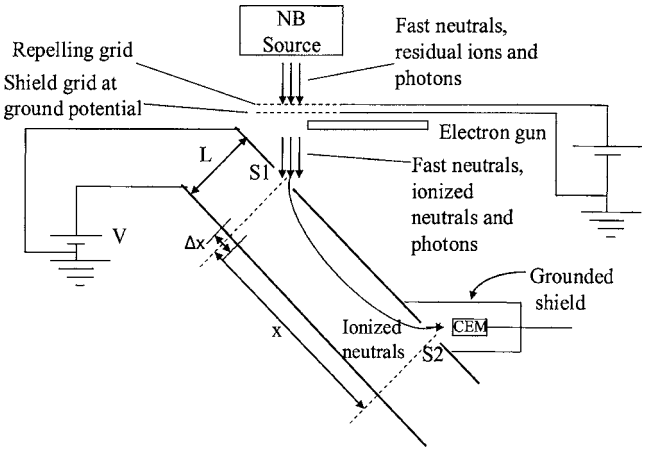

FIG. 4. Schematic of parallel-plate electrostatic ion energy analyzer.

plate analyzer hereafter) together with a channel electron multiplier (CEM) (model 5904 Magnum, Burle Electro-Optics Inc.) was used to measure the ion energy distribution. A schematic of the parallel-plate analyzer is shown in Fig. 4. It was a modified version of a design proposed by Yarnold and Bolton,[19] and elaborated on by Harrower.[20] The principle of operation is that the path of a charged particle in an electric field depends on the particle's energy. A uniform electric field was created by applying a variable voltage between the two parallel metal plates. The upper plate was held at ground potential and the lower plate was kept at positive dc potential (V) with respect to ground (model N5752A, Agilent Technologies). The upper plate had an entrance slit (S1) and an exit slit (S2). The CEM was mounted in front of the exit slit. Ions pass through the entrance slit and travel in parabolic trajectories, covering different horizontal distances depending on the initial ion kinetic energy and applied voltage between the plates. The exit slit, S2, placed at a suitable distance x from the entrance slit, S1, works as an energy selector, allowing a beam of ions of any desired energy to leave the analyzer. Ions exiting slit S2 strike the input aperture of the CEM. The kinetic energy of the ions coming out of S2, E, is related to the potential difference between the plates, V, by[19]

$$E = \frac{Vx}{2L}\frac{1}{\sin 2\theta}. \tag{1}$$

Here, θ is the angle between the ion beam and the plates, and L is the separation between the plates. The dispersion of ions is maximum at θ=45°. At that angle, Eq. (1) becomes

$$E = \frac{Vx}{2L}. \tag{2}$$

Equation (2) establishes a linear relationship between the voltage applied between the plates and the energy of ions able to pass through the exit slit. The energy distribution of ions was obtained by measuring the current collected by the CEM when the voltage between the plates was varied. The resolution of the parallel-plate analyzer is given by[19]

$$\frac{\Delta E}{E} = \frac{\Delta x}{x}, \tag{3}$$

where Δx is the slit width.

The analyzer used in this study consisted of two stainless steel plates, each 15×15 cm^2, separated by a distance of 2.28 cm. Both entrance and exit slits were 2 mm wide and 10 mm long and were separated by 5 cm. The theoretical resolution of this analyzer is 25. The CEM entrance was 2 mm away from the exit slit. The input aperture and the collector end of the CEM were biased at high negative voltage (1.5 kV) and at ground potential, respectively. The CEM was enclosed in a metal cage at ground potential to prevent stray ions and electrons reaching the input aperture of the CEM, as well as to shield the electron beam emanating from the electron gun from the high voltage applied to the input aperture of the CEM.

D. Experimental procedures

1. Plasma ignition

The plasma was ignited at a rf power of 150 W and a pressure of 50 mTorr. Pressure was then set to any desired value by adjusting the feed gas flow rate. Tuning of the matching network minimized the reflected power to almost zero.

2. Measurement of energy distribution of fast neutrals and residual ions

The potential of the repelling grid was set at ground. The voltage of the lower plate of the parallel-plate analyzer was varied linearly and was controlled by a computer through LABVIEW™ via a GPIB data acquisition (DAQ) card. The current from the CEM (representing number of ions per energy interval) was detected with a picoammeter (model 485, Keithley) and was recorded on a computer via a DAQ card. A LABVIEW™ program was used for data acquisition.

To obtain the energy distribution of fast neutrals, a high positive voltage was applied on the repelling grid. Even after removing all residual ions, however, a large background, of the order of 100 times the ionized neutral signal, was observed at the output of the CEM due to UV light and stray ions. By pulsing the electron beam and using a phase sensitive detector (lock-in amplifier, model SR530, Stanford Research), a signal of $\sim 10^{-13}$ A was extracted from ionized fast neutrals. A schematic of the pulsed beam technique used in this study is shown in Fig. 5.

At a downstream chamber pressure of $\sim 10^{-5}$ Torr, there are also slow (thermalized) neutrals present in the chamber. The electron beam ionizes these slow neutrals as well, contributing to the lock-in amplifier signal. To account for this contribution, the procedure described in the previous section was repeated with the plasma off, and this signal was subtracted from the signal with the plasma on.

Equation (3) implies that the width ΔE of the energy of ions coming out from the exit slit of the analyzer is directly proportional to the mean energy E of these ions. Therefore, the ion energy distribution was obtained by dividing the or-

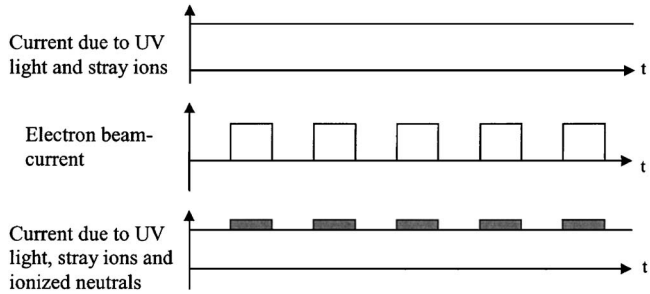

FIG. 5. Using a pulsed electron beam to extract the signal due to ionized fast neutrals from a large background signal.

dinate of the experimental curve by the corresponding energy. Also, the efficiency of ionization of fast neutrals depends on the speed of the neutrals. Faster neutrals ionize less efficiently, giving less signal. Therefore, the ordinate of the experimental curve was multiplied by the velocity of the fast neutrals to obtain the actual energy distribution of the neutral beam.

III. RESULTS AND DISCUSSION

Experiments were conducted over the (plasma gas) pressure range of 10–40 mTorr, power range of 150–350 W, and boundary voltage range of 10–70 V. The reported power is the sum total of the power dissipated in the plasma and the power dissipated in the induction coil. Electron temperature was in the range of 3–6 eV and plasma density was in the range of 1.4×10^{11} to 3.5×10^{12} cm^{-3} for argon plasma, as measured by Kim and Economou[21] in a similar plasma reactor. The base conditions in all the experiments were plasma gas pressure of 10 mTorr, power of 150 W, and boundary voltage V_b of 50 V. Collisions with background slow neutrals change the energy distribution of fast neutrals, residual ions, and ions produced by ionization of neutrals. The plasma chamber used in this study was pumped through the UHV downstream chamber. When the plasma gas pressure was 10 mTorr, with a 1 in. diameter aperture of the neutralization grid, the downstream chamber pressure was $\sim10^{-4}$ Torr. To avoid collisions of fast neutrals with the background gas, the neutralization grid aperture was reduced to 5 mm diameter. In this case, with a plasma gas pressure of 10 mTorr, the downstream chamber pressure was $\sim10^{-5}$ Torr, resulting in a mean free path of $\sim$3 m for argon. The path length of fast neutrals from the neutralization grid to the CEM was about 10 cm. Thus, there should be negligible collisions of fast neutrals with the background gas.

With a smaller aperture neutralization grid, the flow rate into the plasma chamber was also smaller for a given plasma gas pressure (compared to the larger aperture grid). With a small gas flow rate, contamination by outgassing of the alumina walls of the plasma source, as well as sputtering of the walls, could be significant. A spectrum of plasma emission at very low flow rates [0.5 SCCM (SCCM denotes cubic centimeter per minute at STP)] showed that the O- and Al-atom lines were very weak as compared to Ar lines, suggesting that plasma contamination was not important.

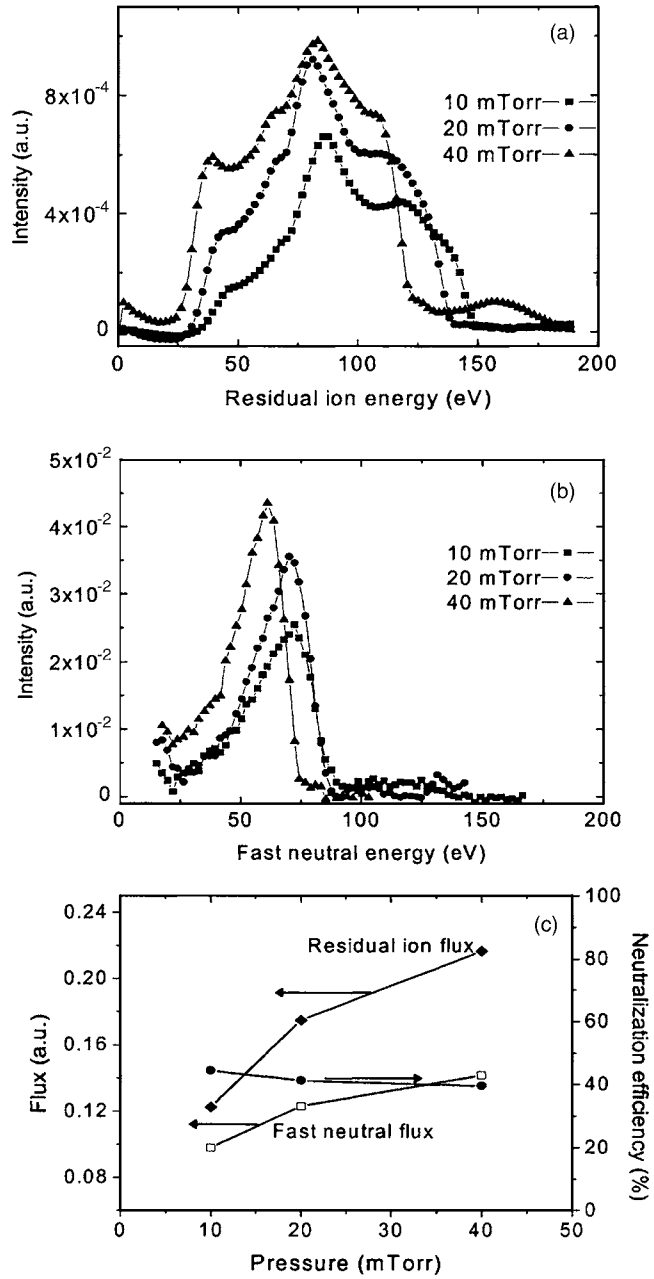

FIG. 6. (a) Residual ion energy distribution. (b) Fast neutral energy distribution. (c) Residual ion flux, fast neutral flux, and neutralization efficiency. Conditions: 150 W power and 50 V boundary voltage. The hole diameter was 154 μm and the hole aspect ratio was 7:1.

Figures 6(a) and 6(b) show the residual IED and fast NED, respectively, for neutralization grid 1 (Table I) for different (plasma gas) pressures. The IED exhibits multiple peaks, suggesting that the ion transit time through the sheath is comparable to the applied rf period. The maximum sheath potential is determined by capacitive coupling by the beam acceleration electrode (Fig. 1) and/or the rf induction coil. In the absence of collisions in the sheath, the maximum ion energy will equal the maximum sheath voltage, if ions follow the instantaneous sheath potential. The sheath thickness was estimated by Kim and Economou[21] in a similar reactor to be in the range 360–380 μm, at 150 W and 10–40 mTorr. The

ion-atom charge transfer cross section for Ar ions at 90 eV is 3.0×10^{-15} cm^2.[22] Thus the ion mean free path at 10, 20, and 40 mTorr is 10, 5, and 2.5 mm, respectively, making ion flow in the sheath nearly collisionless. Since the sheath thickness is larger than the hole diameter, $L_{sh}>d$, there should be only weak plasma molding in the holes.[23] Thus, ions should collide with the inside surface of the holes of the grid at a grazing angle, based on their angular distribution coming out of the plasma, augmented by plasma molding over the holes. The peak of the NED is shifted to lower energies by 20 eV, compared to that of the IED. Helmer and Graves[24] have reported a surface interaction model (for a "smooth" surface) with an energy exchange given by

$$\sqrt{\frac{\varepsilon_r}{\varepsilon_i}}=\left(\frac{\mu}{\mu+1}\right)^2\left(\cos\chi_{1/2}+\sqrt{\frac{1}{\mu^2}-\sin^2\chi_{1/2}}\right)^2,$$

$$\chi_{1/2}=\frac{\pi}{2}-\vartheta_i,\quad \mu=\frac{m_{\mathrm{Ar}}}{m_{\mathrm{wall}}}. \tag{4}$$

Here ε_i and ε_r are the kinetic energy of the incident ion and reflected atom, respectively, ϑ_i is the incident angle, and m_{Ar} and m_{wall} are the mass of the argon atom and the wall material atom, respectively. Using this expression for ions with 92 eV (peak energy for grid 1 at 10 mTorr pressure, 50 V boundary voltage, and 150 W power) and an assumed 5° divergence, ($\vartheta=85°$), a shift of only 2 eV is predicted for the scattered neutrals. This is much less than the energy shift obtained experimentally [compare Figs. 6(a) and 6(b)]. The most likely reason is roughness of the surface of the grid holes. Also, high energy ions have smaller angular spread (less affected by plasma molding) and may go through the hole without collision. Lower energy ions are more likely to be affected by plasma molding, and to divert and strike the sidewall, turning into neutrals. Therefore the neutral energy distribution will be weighted more heavily by these lower energy ions. The NED shows a large increase at very low energies due to ionization of the background gas, and numerical artifacts introduced by dividing the ordinate by $\sqrt{E}$, to correct for the velocity dependence of the ionization efficiency of the neutrals. As pressure increases, the energy distributions of residual ions and fast neutrals shift towards lower energies [Figs. 6(a) and 6(b), respectively], since the electron temperature and thus the sheath potential decrease. The full width at half maximum of the ion and neutral energy distributions is almost independent of pressure. Woodworth *et al.*[25] made similar observations for the IEDs in their ICP system.

Helmbrecht[26] used calorimetry to measure the heat flux due to fast neutrals and fast neutrals plus ions as 6 and 18 mW/cm^2, respectively, for grid 1 at a pressure of 10 mTorr, power of 150 W, and V_b of 50 V. To obtain the relative ion and fast neutral fluxes, these values must be divided by the mean energy of ions and neutrals, respectively. The mean energy was calculated by

$$\langle E\rangle=\frac{\int_0^\infty f(E)E\,dE}{\int_0^\infty f(E)\,dE}. \tag{5}$$

Here, E is the energy and $f(E)$ is the measured energy distribution. The mean energies of ions and neutrals were found to be 98 and 61 eV, respectively, yielding the fluxes shown in Fig. 6(c). Both the ion and neutral fluxes increase with pressure. The neutralization efficiency, defined as the ratio of the fast neutral flux to the total (fast neutral plus residual ion) flux, is nearly independent of pressure. This is an indication that neutralization is by surface processes and not by charge exchange with slow neutrals in the gas phase.

Figures 7(a) and 7(b) show the IED and NED for different power levels, for grid 1. The peak and minimum ion and neutral energies are nearly constant, while the maximum energy increases with power. For a sheath potential (equal to the plasma potential over the grounded neutralization grid) of the form $V_p=V_{\mathrm{dc}}+V_{\mathrm{rf}}\sin(2\pi ft)$, when the ion transit time across the sheath is much shorter than the rf period, the energy spread due to rf modulation is given by[27–29]

$$\Delta E=\left(\frac{4eV_{\mathrm{rf}}}{3\pi fL_{\mathrm{sh}}}\right)\left(\frac{2eV_{\mathrm{dc}}}{m}\right)^{1/2}. \tag{6}$$

At 150, 250, and 350 W, the estimated sheath thickness is equal to 375, 275, and 200 μm, respectively. As power increases, L_{sh} decreases, while both V_{rf} and V_{dc} tend to increase. Therefore ΔE increases. Also, as power increases, plasma density increases, causing an increase in ion flux crossing the plasma-sheath boundary and entering the holes of the neutralization grid. Thus, the sum of outcoming residual ion flux and fast neutral flux increases with power. However, as power increases, the sheath thickness decreases, resulting in more plasma molding and a larger fraction of the ion flux neutralized by collisions with the neutralization grid. Thus the ion flux does not increase with power, while the fast neutral flux increases drastically with power [see Fig. 7(c)]. As a result, the neutralization efficiency also increases with power [Fig. 7(c)].

Figures 8(a) and 8(b) show the IED and NED, respectively, for grid 1, with boundary voltage V_b as the parameter. The plasma potential increases as V_b increases, resulting in more energetic ions entering the neutralization grid holes. Hence the energy of both residual ions and fast neutrals increases with boundary voltage. Also, as V_b increases, L_{sh} increases as well, and plasma molding becomes weaker, making ion flow through the grid holes more directional. Directional ions are less likely to collide with the grid, and the residual ion flux increases with V_b [see Fig. 8(c)]. The fast neutral flux also increases slightly, and this might seem unexpected at first. If fewer ions neutralize, the fast neutral flux should decrease with V_b. However, the parallel-plate analyzer records only directional particles. As L_{sh} increases, the directionality of fast neutrals also increases, and the ob-

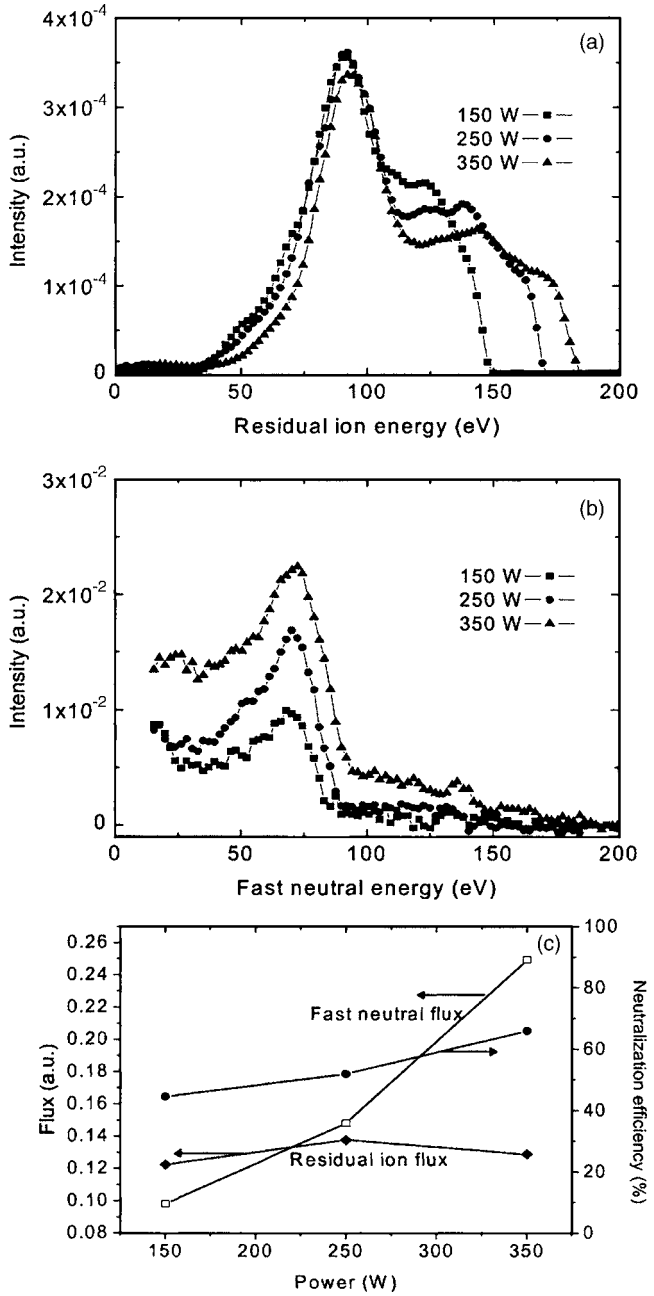

FIG. 7. (a) Residual ion energy distribution. (b) Fast neutral energy distribution. (c) Residual ion flux, fast neutral flux, and neutralization efficiency. Conditions: 10 mTorr pressure and 50 V boundary voltage. The hole diameter was 154 μm and the hole aspect ratio was 7:1.

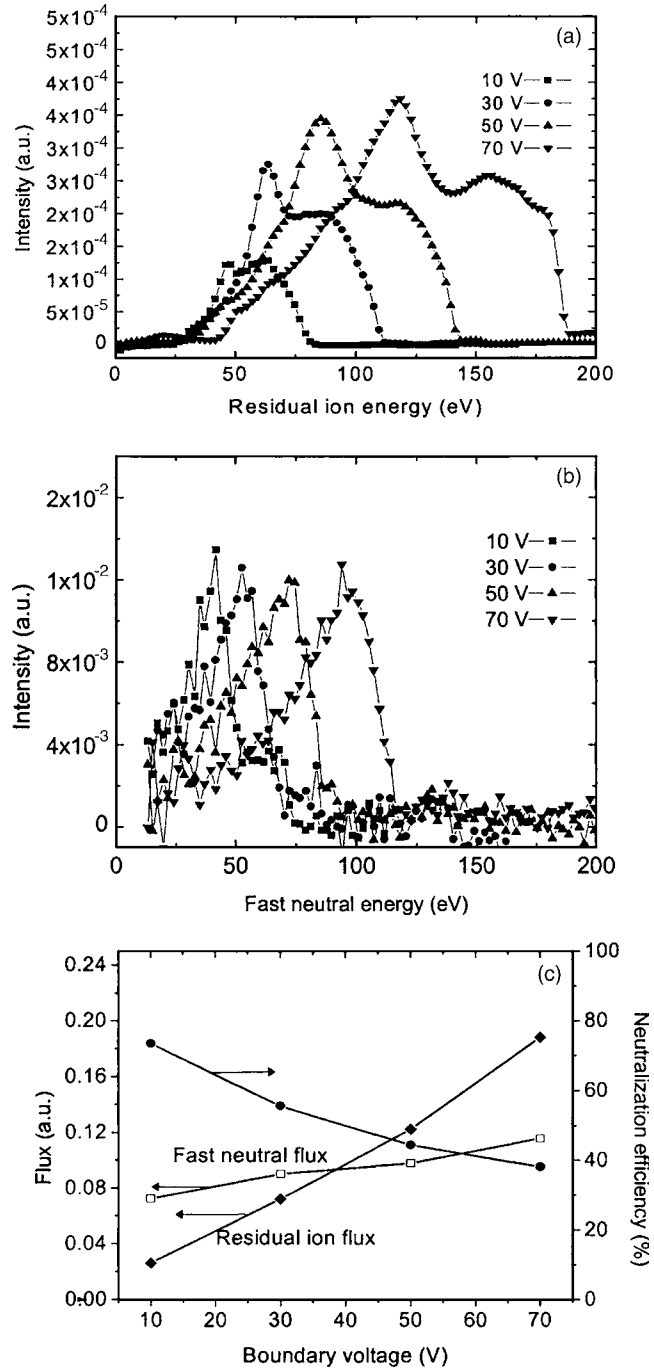

FIG. 8. (a) Residual ion energy distribution. (b) Fast neutral energy distribution. (c) Residual ion flux, fast neutral flux, and neutralization efficiency. Conditions: 150 W power and 10 mTorr pressure. The hole diameter was 154 μm and the hole aspect ratio was 7:1.

served neutral flux is higher at higher V_b. The net result is that the neutralization efficiency decreases with V_b.

Figures 9(a) and 9(b) show the IED and NED, respectively, for neutralization grid 2 (Table I), with pressure as the parameter. The NEDs are shifted to even lower energies with respect to the IEDs for grid 2, as compared to grid 1. This is because of more severe molding (due to larger hole diameter) in this case causing ions to strike the walls of the grid at larger angles (off the vertical) and lose more energy. The residual ion flux decreases as pressure increases, in contrast to grid 1 [Fig. 6(c)]. The mean free paths for ion-atom charge transfer collisions at 10, 20, and 40 mTorr are 10, 5, and 2.5 mm, respectively, while the thickness of grid 2 is 2.3 mm. Thus gas-phase charge exchange collisions are likely in this case as ions pass through the neutralization grid holes, reducing ion flux. The fast neutral flux increases correspondingly, and this yields a neutralization efficiency that is an increasing function of pressure [see Fig. 9(c)]. The characteristics of neutralization grids 3 and 4 (Table I) were similar to those of grid 2.

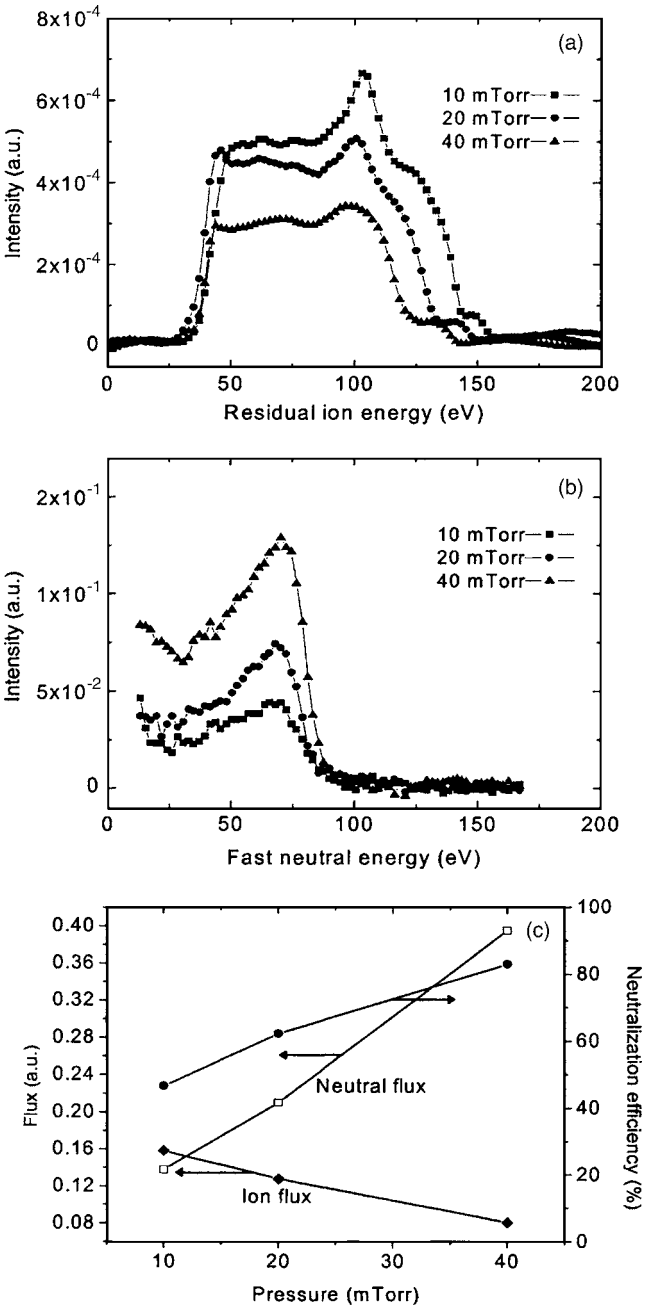

FIG. 9. (a) Residual ion energy distribution. (b) Fast neutral energy distribution. (c) Residual ion flux, fast neutral flux, and neutralization efficiency. Conditions: 150 W power and 50 V boundary voltage. The hole diameter was 330 μm and hole aspect ratio was 10:1.

Figure 10 shows the residual ion and fast neutral fluxes for different grids at a pressure of 10 mTorr, power of 150 W, and boundary voltage of 50 V. The residual ion flux steadily decreases as the diameter of the neutralization grid holes or their aspect ratio increases. As the hole diameter increases, plasma molding becomes more severe, and more of the oncoming ions are diverted to strike the inside surface of the holes and neutralize. For the 330 μm diameter hole, the ion flux decreases by a factor of 1.6 as the aspect ratio (AR) increases from 7:1 (grid 2) to 10:1 (grid 3). In contrast, the fast neutral flux increases as AR increases. Thicker grids

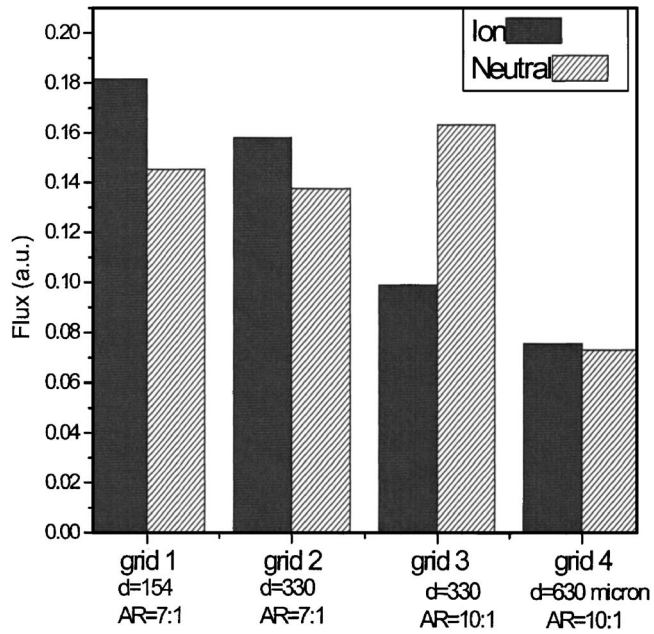

FIG. 10. Residual ion flux and fast neutral flux as a function of hole diameter and hole aspect ratio. Conditions: 10 mTorr pressure, 150 W power, and 50 V boundary voltage.

cause more ions to collide with the walls, creating more fast neutrals. Regarding the hole size dependence, the fast neutral flux increases by going from 154 to 330 μm diameter holes, only to drop as the hole diameter is further increased to 630 μm. For these conditions, the sheath thickness is L_{sh} =370 μm. For a hole diameter of 330 μm, the plasma-sheath interface gently dips in the hole and facilitates formation of fast neutrals. For a 630 μm diameter hole, plasma molding becomes so severe (see Fig. 11) that ions strike the wall at angles large enough for the resulting fast neutrals to be highly divergent. Such divergent neutrals do not make it to the input aperture of the analyzer to be detected. In fact,

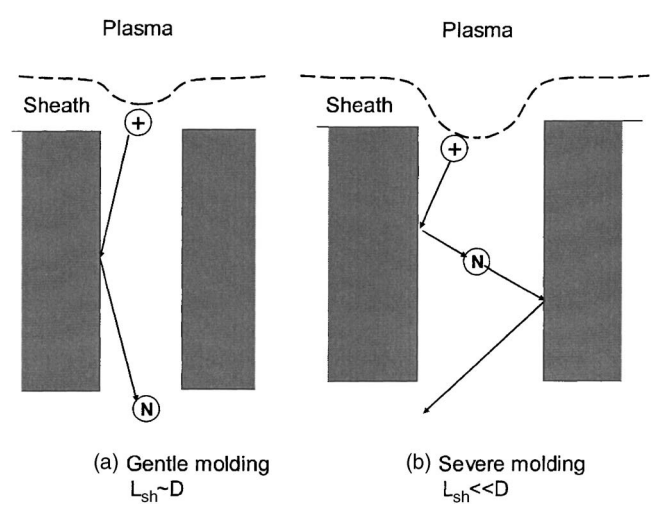

FIG. 11. Schematic of plasma molding over holes with different diameters: (a) gentle molding for a sheath thickness comparable to the hole diameter and (b) severe molding for a sheath thickness much less than the hole diameter.

under these conditions, initially fast neutrals may suffer multiple collisions with the internal wall of the holes, resulting in a very low energy divergent neutral flux which may not be useful for materials processing.

IV. CONCLUSIONS

The energy distribution and flux of fast neutrals and residual ions extracted from a neutral beam source were measured. Neutral beams may be useful for mitigating charging damage in the fabrication of microelectronic devices. An inductively coupled source was used to generate a high density argon plasma. The plasma potential was raised by applying a bias voltage (boundary voltage) to an electrode in contact with the plasma. Positive ions were expelled from the plasma through a metal grid with high aspect ratio holes. Ions suffered grazing angle collisions with the sidewall of the grid holes turning into fast neutrals. The fast neutral energy distribution (NED) was always shifted to lower energies compared to the corresponding residual ion energy distribution (IED). This reflects the energy loss in collisions of ions with the sidewall of the grid holes. The neutralization efficiency (NE), defined as the ratio of the fast neutral flux to the total (residual ion plus fast neutral) flux increased with plasma power and decreased with boundary voltage. The pressure dependence of the NE was more complicated. For thinner grids (1.25 mm thick), the NE was independent of pressure, while for thicker grids the NE increased with pressure, reflecting the influence of charge exchange collisions of ions in their transit through the grid holes. The residual ion current decreased monotonically with increasing hole diameter and hole aspect ratio. Larger holes result in more severe plasma molding, and more ions are diverted to strike the sidewall of the grid holes and neutralize. The fast neutral flux first increased and then dropped as the hole diameter was increased. Large hole diameters yield more ion neutralization and hence a higher fast neutral flux. When the hole diameter becomes much larger than the sheath thickness, however, ions strike the sidewall at large angles (off vertical), yielding a wide angular distribution of the resulting fast neutrals. These off axis neutrals are not detected, and the measured fast neutral flux decreases.

Collisions of ions with the sidewall of the holes are critical for generating fast neutral beams. Scattering of ions off a solid surface depends on ion energy and angle of impact, and also on surface roughness. The surface roughness of the holes of the grids used in the present study was not characterized. Experiments similar to those reported here under well controlled surface roughness conditions will be reported in a future publication.

ACKNOWLEDGMENTS

The authors thank Dr. Nader Sadeghi for helping with the lock-in amplifier measurements. Financial support from the Texas Advanced Technology Program and the National Science Foundation (CTS-0072854 and MII-0303790) is gratefully acknowledged.

[1]S. Samukawa, Appl. Phys. Lett. **64**, 3398 (1994).
[2]N. Fujiwara, T. Maruyama, and M. Yoneda, Jpn. J. Appl. Phys., Part 1 **35**, 2450 (1996).
[3]G. S. Hwang and K. P. Giapis, J. Appl. Phys. **82**, 566 (1997).
[4]D. J. Economou and R. Alkire, J. Electrochem. Soc. **135**, 941 (1988).
[5]J. C. Arnold and H. H. Sawin, J. Appl. Phys. **70**, 5314 (1992).
[6]H. Kuwano and F. Shimokawa, J. Vac. Sci. Technol. B **6**, 1565 (1988).
[7]F. Shimokawa, H. Tanaka, Y. Uenishi, and R. Sawada, J. Appl. Phys. **66**, 2613 (1989).
[8]T. Mizutani and T. Yunogami, Jpn. J. Appl. Phys., Part 1 **29**, 2220 (1990).
[9]T. Yunogami, K. Yogokawa, and T. Mizutani, J. Vac. Sci. Technol. A **13**, 952 (1995).
[10]K. Yokogawa, T. Yunigami, and T. Mizutani, Jpn. J. Appl. Phys., Part 1 **35**, 1901 (1996).
[11]T. Tsuchizawa, Y. Jin, and S. Matsuo, Jpn. J. Appl. Phys., Part 1 **33**, 2200 (1994).
[12]Y. Jin, T. Tsuchizawa, and S. Matsuo, Jpn. J. Appl. Phys., Part 2 **34**, 465 (1995).
[13]S. Panda, D. J. Economou, and L. Chen, J. Vac. Sci. Technol. A **19**, 398 (2001).
[14]S. Samukawa, K. Sakamoto, and K. Ichiki, J. Vac. Sci. Technol. A **20**, 1566 (2002).
[15]S. Noda, H. Nishimori, T. Iida, T. Arikado, K. Ichiki, T. Ozaki, and S. Samukawa, J. Vac. Sci. Technol. A **22**, 1506 (2004).
[16]H. Ohtake, N. Inoue, T. Ozaki, and S. Samukawa, J. Vac. Sci. Technol. B **23**, 210 (2005).
[17]D. Kim and D. J. Economou, IEEE Trans. Plasma Sci. **30**, 2048 (2002).
[18]R. C. Wetzel, F. A. Baiocchi, T. R. Hayes, and R. S. Freund, Phys. Rev. A **35**, 559 (1987).
[19]G. D. Yarnold and H. C. Bolton, Rev. Sci. Instrum. **26**, 38 (1949).
[20]G. A. Harrower, Rev. Sci. Instrum. **26**, 850 (1955).
[21]C.-K. Kim and D. J. Economou, J. Appl. Phys. **91**, 2594 (2002).
[22]E. W. McDaniel, J. B. A. Mitchell, and M. E. Rudd, *Atomic Collisions: Heavy Particles Projectiles* (Wiley, New York, 1993).
[23]D. Kim and D. J. Economou, J. Vac. Sci. Technol. B **21**, 1248 (2003).
[24]B. A. Helmer and D. B. Graves, J. Vac. Sci. Technol. A **16**, 3502 (1998).
[25]J. R. Woodworth, M. E. Riley, D. C. Meister, B. P. Aragon, M. S. Lee, and H. H. Sawin, J. Appl. Phys. **80**, 1304 (1996).
[26]C. Helmbrecht, M.S. thesis, University of Applied Sciences, 2005.
[27]P. Beniot-Cattin and L. C. Bernard, J. Appl. Phys. **39**, 5723 (1969).
[28]Y. Okamoto and H. Tamagawa, J. Phys. Soc. Jpn. **27**, 270 (1969).
[29]Y. Okamoto and H. Tamagawa, J. Phys. Soc. Jpn. **29**, 187 (1970).